Molecular Crystals and Liquid Crystals Incorporating Nonlinear Optics

Publication details, including instructions for authors and subscription information:
http://www.tandfonline.com/loi/gmcl17

Effects of Anchoring Under Intense Optical Fields in a Cholesteric Liquid Crystal

J.-C. Lee [a], A. Schmid [a] & S. D. Jacobs [a]

[a] Laboratory for Laser Energetics, University of Rochester, 250 East River Road, Rochester, New York, 14623-1299

Version of record first published: 22 Sep 2006.

To cite this article: J.-C. Lee , A. Schmid & S. D. Jacobs (1989): Effects of Anchoring Under Intense Optical Fields in a Cholesteric Liquid Crystal, Molecular Crystals and Liquid Crystals Incorporating Nonlinear Optics, 166:1, 253-265

To link to this article: http://dx.doi.org/10.1080/00268948908037154

Mol. Cryst. Liq. Cryst., 1989, Vol. 166, pp. 253–265
Reprints available directly from the publisher
Photocopying permitted by license only

Printed in the United States of America

Effects of Anchoring Under Intense Optical Fields in a Cholesteric Liquid Crystal

J.-C. LEE, A. SCHMID and S. D. JACOBS

Laboratory for Laser Energetics, University of Rochester, 250 East River Road, Rochester, New York 14623-1299

(*Received June 15, 1988*)

In this paper, we show theoretically how the anchoring conditions at the substrate-cholesteric liquid crystal fluid interface affect the pitch change of a cholesteric liquid crystal in an intense optical field. Strong anchoring at both cell interfaces gives rise to pitch dilation and contraction, while strong input-side/weak output-side anchoring results in pitch dilation only. Weak input-side/strong output-side anchoring creates pitch contraction.

I. INTRODUCTION

Cholesteric liquid crystals (CLC) have been used as polarizers, bandpass and notch filters, mirrors, apodizers, and optical isolators.[1-3] These are all based on the linear propagation of light through the medium. In this case, the changes of the liquid crystal helical structure due to an optical field are almost negligible. But in intense optical fields, the helical structure can be changed and nonlinear effects can occur. In this case, the anchoring conditions between substrates and CLC fluid play a dominant role. In 1982, H. G. Winful[4] solved the coupled Euler-Lagrange and Maxwell's equations to show theoretically how optical bistability develops as a result of pitch dilation in a CLC with strong anchoring at the input side. In 1987, we showed theoretically[5] that under exposure to a plane wave with a Gaussian intensity distribution, a retro-self-focusing effect occurs in which the reflected field comes to a focus. This is accompanied by a pinholing effect in which the retro-self-focusing effect occurs within a diameter $\sqrt{2}w$, where $2w$ is the spot size of an incident Gaussian beam. These effects were experimentally proven in a CLC-dielectric resonator, where a CLC was used as a laser-resonator end mirror.

Normally a CLC cell with a planar structure is prepared between two flat substrates as shown in Figure 1. In this figure, z is the light propagation direction and L is the total CLC fluid thickness. In our previous experiments,[6] we used a CLC with strong input-side/weak output-side surface anchoring at $z = 0$ and at $z = L$, respectively (in abbreviation CLC-10) or a CLC with strong input-side/strong out-

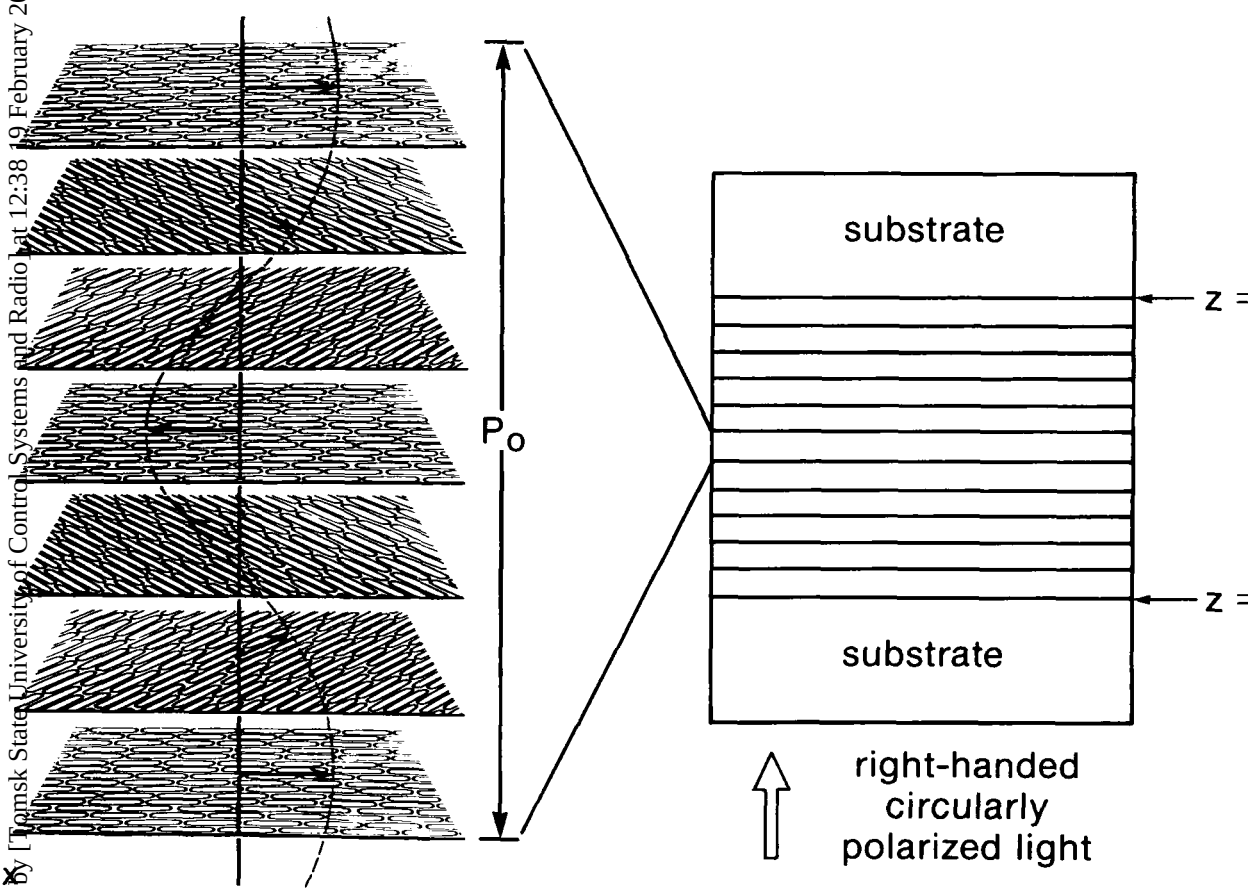

FIGURE 1 Schematic diagram of a cholesteric liquid crystal cell. The left-hand side of the figure shows one pitch length of the helical structure in the CLC. Arrows within each plane indicate director orientation.

put-side surface anchoring (CLC-11). Both devices showed the retro-self-focusing and pinholing effects. However, we were not successful in obtaining stimulated emission in a laser resonator for a CLC with weak input-side/strong output-side (CLC-01) or weak input-side/weak output-side (CLC-00) surface anchoring. One reason for this is that the molecular order for the planar helix structure does not extend over macroscopic dimensions unless some anchoring in the form of rubbing on the substrate is provided. This creates a preferred direction at the substrate-CLC fluid interface and good alignment through the medium of moderate thickness. Weak anchoring causes an increase in scatter-related losses. In the fabrication of a CLC, strong surface anchoring between substrates and the CLC fluid at both sides gives rise to good alignment in the CLC cell. A better understanding of the relationship between anchoring and performance, especially for a CLC-11 configuration, is essential for further development of CLC resonator mirror optics.

In this paper, we will solve the coupled-Lagrange and Maxwell's equations for the case of CLC-11 and show that pitch dilation and contraction occur simultaneously in separate CLC regions. We will then discuss the differences between the CLC-10 and CLC-11 conditions by comparing the relationship between incident and transmitted field intensity, as well as comparing reflectivity and phase shift.

II. THEORY

Let us consider a right-handed CLC-11 cell as shown in Figure 1 whose helix axis is oriented along the z-axis. The helical structure of the CLC can be described by the director $\hat{n}(z)$ which represents the average orientation of the elongated liquid-crystal molecules. Arrows within each plane indicate the director orientation, and the pitch P_o is the distance required for the director to rotate by 360°. Its cartesian components are:

$$n_x = \cos\theta(z),\ n_y = \sin\theta(z),\ n_z = 0 \tag{1}$$

In the absence of external fields, the angle $\theta(z)$ is given by $\theta = q_o z$, where q_o is the unperturbed wave number of the helix whose pitch is $P_o = 2\pi/q_o$.

When right-handed circularly polarized light propagates along the z-axis, the total electric field $\mathbf{E}$ in the medium can be described by circularly polarized components as follows:

$$\mathbf{E} = \mathrm{Re}[\{E_+(z)(\hat{x} - i\hat{y})/\sqrt{2} + E_-(z)(\hat{x} + i\hat{y})/\sqrt{2}\}\, e^{-i\omega t}] \tag{2}$$

where $E_\pm = (E_x \pm E_y)/\sqrt{2}$. The first term in Eq. (2) represents a forward-propagating wave and the second term represents a counter-propagating wave which has the same sense of polarization as the forward-propagating wave.

The electric displacement, $\mathbf{D}$, of the medium is given by[7]

$$\mathbf{D} = \hat{\epsilon}(z)\mathbf{E} = \epsilon_\perp \mathbf{E} + \epsilon_a \hat{n}(\hat{n} \cdot \mathbf{E}) \tag{3}$$

where $\epsilon_a = \epsilon_\parallel - \epsilon_\perp$ is the optical dielectric anisotropy and $\epsilon_\parallel$ and $\epsilon_\perp$ represent the dielectric constant parallel and perpendicular to the local director. The explicit form of the dielectric tensor matrix is

$$\hat{\epsilon} = \epsilon_{av}\begin{pmatrix}1, & 0\\ 0, & 1\end{pmatrix} + \frac{\epsilon_a}{2}\begin{pmatrix}\cos 2\theta(z), & \sin 2\theta(z)\\ \sin 2\theta(z), & -\cos 2\theta(z)\end{pmatrix} \tag{4}$$

where $\epsilon_{av} = (\epsilon_\parallel + \epsilon_\perp)/2$ is the average dielectric constant. Then Maxwell's equation in the medium can be rewritten as

$$-\frac{d^2\mathrm{E}_\pm}{dz^2} = k_o^2\mathrm{E}_\pm + k_1^2\mathrm{E}_\mp e^{\pm i2\theta(z)}. \tag{5}$$

where $k_o^2 = (\omega/c)^2\epsilon_{av}$ and $k_1^2 = (\omega/c)^2\epsilon_a/2$. The new orientation of the director $\theta(z)$ in Equation (5) can be found by minimizing the free energy F under the external electric field **E**.

$$\mathrm{F} = \int_v d^3r\frac{1}{2}\{k_{11}(\nabla\cdot\hat{n})^2 + k_{22}(\hat{n}\cdot\nabla x\hat{n} + q_o)^2 + k_{33}(\hat{n}x\nabla x\hat{n})^2 - \mathbf{E}\cdot\mathbf{D}/4\pi\} \tag{6}$$

where k_{11}, k_{22} and k_{33} are the Frank elastic constants that describe the basic distortions of splay, twist, and bend, respectively. This leads to the Euler-Lagrange equation of motion for the director angle $\theta(z)$:

$$\frac{d^2\theta}{dz^2} = \frac{\epsilon_a}{16\pi k_{22}}[\mathrm{Re}(\mathrm{E}_+\mathrm{E}_-^*)\sin 2\theta - \mathrm{Im}(\mathrm{E}_+\mathrm{E}_-^*)\cos 2\theta] \tag{7}$$

As a trial solution, the forward-propagating and counter-propagating fields can be represented as

$$\mathrm{E}_\pm = |\epsilon_\pm(z)|\exp[i\phi_\pm(z) \pm iq_o z] \tag{8}$$

By substituting Eq. (8) into Eq. (5), Maxwell's equation is reduced to a coupled amplitude equation within the slowly-varying-envelope approximation

$$\frac{d|\epsilon_+|}{dz} = \kappa|\epsilon_-|\sin\Psi \tag{9}$$

$$\frac{d|\epsilon_-|}{dz} = \kappa|\epsilon_+|\sin\Psi \tag{10}$$

$$\frac{d\Psi}{dz} = 2(q_o + \Delta k) + \kappa(|\epsilon_-|/|\epsilon_+| + |\epsilon_+|/|\epsilon_-|)\cos\Psi - 2\frac{d\theta}{dz} \tag{11}$$

where $\Psi(z) = \phi_+(z) - \phi_-(z) + 2q_o z - 2\theta(z)$, the coupling coefficient $\kappa = k_1^2/2q_o$, and the detuning parameter $\Delta k = (k_o^2 - q_o^2)/2q_o$. We now proceed to solve Eqs. (9), (10), and (11) for different boundary conditions.

(A) CLC-10 Case

This case was discussed by H. G. Winful.[4] For this case, the boundary conditions required are as follows:

$$|\epsilon_+(L)| = |\epsilon_T| \quad \text{, transmitted field at } z = L \tag{12}$$

$$|\epsilon_-(L)| = 0 \quad \text{, no reflection at } z = L \tag{13}$$

$$\left.\frac{d\theta}{dz}\right|_{z=L} = q_o \quad \text{, weak anchoring at } z = L \tag{14}$$

$$\theta(0) = 0 \quad \text{, strong anchoring at } z = 0 \tag{15}$$

Substituting Eq. (8) into Eq. (7), we have

$$\frac{d^2\theta}{dz^2} = \frac{\epsilon_a}{16\pi k_{22}\kappa}\frac{d|\epsilon_+|^2}{dz} \tag{16}$$

Integration of Eq. (16) with the boundary condition in Eq. (14), gives

$$q(z) = \frac{d\theta}{dz} = q_o - \frac{\epsilon_a}{16\pi k_{22}\kappa}(|\epsilon_+(z)|^2 - |\epsilon_T|^2) \tag{17}$$

Since $|\epsilon_+(z)|^2 > |\epsilon_T|^2$, $q(z) < q_o$. In other words, the pitch dilates in proportion to the local field intensity.

(B) CLC-01 Case

For this case, only the boundary condition in Eq. (14) is changed.

$$\left.\frac{d\theta}{dz}\right|_{z=0} = q_o \quad \text{, weak anchoring at } z = 0 \tag{18}$$

This boundary condition leads to

$$q(z) = q_o - \frac{\epsilon_a}{16\pi k_{22}\kappa}(|\epsilon_+(z)|^2 - |\epsilon_+(0)|^2) \tag{19}$$

Since $|\epsilon_+(0)|^2 > |\epsilon_+(z)|^2$, $q(z) < q_o$, that is, pitch contraction will occur.

(C) CLC-11 Case

For a CLC-11, the following boundary conditions are required.

$$|\epsilon_+(L)| = |\epsilon_T| \quad \text{, the transmitted field amplitude at } z = L \tag{20}$$

$$|\epsilon_-(L)| = 0 \quad \text{, no reflection at } z = L \tag{21}$$

From Eq. (1),

$$\theta(0) = 0 \quad \text{, the director angle at } z = 0 \tag{22}$$

$$\theta(L) = q_o L \quad \text{, the director angle at } z = L \tag{23}$$

In addition to the above boundary conditions, the helix wave number should be equal to q_o at some point $z = a$ inside the medium, that is,

$$q(z = a) = \left.\frac{d\theta}{dz}\right|_{z=a} = q_o. \tag{24}$$

Integration of Eq. (16) with the boundary condition in Eq. (24), gives

$$q(z) = q_o - \frac{\epsilon_a}{16\pi k_{22}\kappa}\{|\epsilon_+(z)|^2 - |\epsilon_+(a)|^2\}. \tag{25}$$

When $0 \le z < a$, $q(z) < q_o$, that is, the pitch dilates in proportion to the optical field intensity ($\epsilon_a > 0$) and $q(z) = q_o$ at $z = a$. When $a < z \le L$, $q(z) > q_o$, that is, pitch contraction occurs. Therefore pitch dilation and contraction occur simultaneously in a CLC-11. From Eq. (9), (10), (11), and (25), we find

$$\frac{d}{dz}(|\epsilon_+\epsilon_-|\cos\Psi) = -\frac{1}{\kappa}\frac{d|\epsilon_+|^2}{dz}\left[\Delta k + \frac{\epsilon_a}{16\pi k_{22}\kappa}\{|\epsilon_+(z)|^2 - |\epsilon_+(a)|^2\}\right] \tag{26}$$

Let $u(z) = \gamma|\epsilon_+(z)|^2$, $J = \gamma|\epsilon_T|^2$, $S = \gamma|\epsilon_+(a)|^2$, and $v(z) = \gamma|\epsilon_-(z)|^2$ where $\gamma = \epsilon_a/32\pi k_{22}\kappa^2$.

From the boundary conditions Eq. (20) and (21), $u(L) = J$ and $v(L) = 0$ respectively. Then Eq. (26) becomes

$$\sqrt{uv}\cos\Psi = -(u - J)\{\Delta k/\kappa - 2S + u + J\}. \tag{27}$$

Multiplying Eq. (9) by $|\epsilon_+(z)|$ and rearranging it, we have

$$\frac{d|\epsilon_+|^2}{dz} = 2\kappa|\epsilon_+\epsilon_-|\sin\Psi. \tag{28}$$

Substituting Eq. (27) into Eq. (28), one finds

$$\frac{du}{dz} = -2\kappa\sqrt{Q(u)} \tag{29}$$

where $Q(u) = (u - J)\{u - (u - J)(\Delta k/\kappa - 2S + u + J)^2\}$.

Integrating Eq. (25) and using the boundary condition in Eq. (22), we have

$$\theta(z) = (q_o + 2\kappa S)z - 2\kappa \int_o^z u(z)dz. \tag{30}$$

The boundary condition $\theta(L) = q_o L$ in Eq. (23) provides a means to calculate the normalized intensity S in Eq. (29), as follows:

$$S = \frac{1}{L}\int_o^L u(z)dz. \tag{31}$$

The physical interpretation of S is the average normalized intensity in the medium, where the helix wave number is equal to q_o.

When the roots of $Q(u)$ are real and $u_1 > u_2 > u_3 > u_4$, Eq. (29) may be solved in terms of a Jacobian elliptic function[8]

$$u(z) = u_3 + \frac{u_2 - u_3}{1 - (u_1 - u_2)(u_1 - u_3)^{-1}\,\mathrm{Sn}^2[2\kappa(z - L)/g, k]} \tag{32}$$

where Sn is a Jacobian elliptic function with $g = 2/[(u_1 - u_3)(u_2 - u_4)]^{1/2}$ and $k = [(u_1 - u_2)(u_3 - u_4)]^{1/2}g/2$. When the two roots u_1 and u_2 of $Q(u)$ are real and $u_1 \geq u \geq u_2$ and the two roots u_3 and u_4 are complex, the solution of Eq. (29) becomes

$$u(z) = \frac{Bu_1 + Au_2 + (Au_2 - Bu_1)Cn[2\kappa(z - L)/g,k]}{A + B + (A - B)\,Cn[2\kappa(z - L)/g,k]} \tag{33}$$

where $A^2 = (u_1 - b_1)^2 + b_2^2$, $B^2 = (u_2 - b_1)^2 + b_2^2$, $b_1 = \mathrm{Re}[u_3]$ and $b_2 = \mathrm{Im}[u_3]$, and Cn is a Jacobian elliptic function with $g = 1/\sqrt{AB}$ and $b_2 = \{(u_1 - u_2)^2 - (A - B)^2\}/4AB$.

A plot of the normalized intensity $u(z)$ for the forward-propagating wave in the CLC medium is shown in Figure 2. In this figure, $\kappa L = 2.0$, $q_o L = 10\,\pi$, and $J = 0.08$. The solid lines represent the normalized intensity $u(z)$ for CLC-11. The incident field intensity $u(z)$ decays almost exponentially along the z-axis. The dotted lines represent the normalized intensity $u(z)$ for CLC-10. Additional input intensity is required to have the same transmitted intensity J for CLC-11 because the strong anchoring at $z = L$ impedes the helical structure from changing. The value S on the ordinate represents the average normalized intensity in the medium, where the helix wave number of the CLC equals q_o.

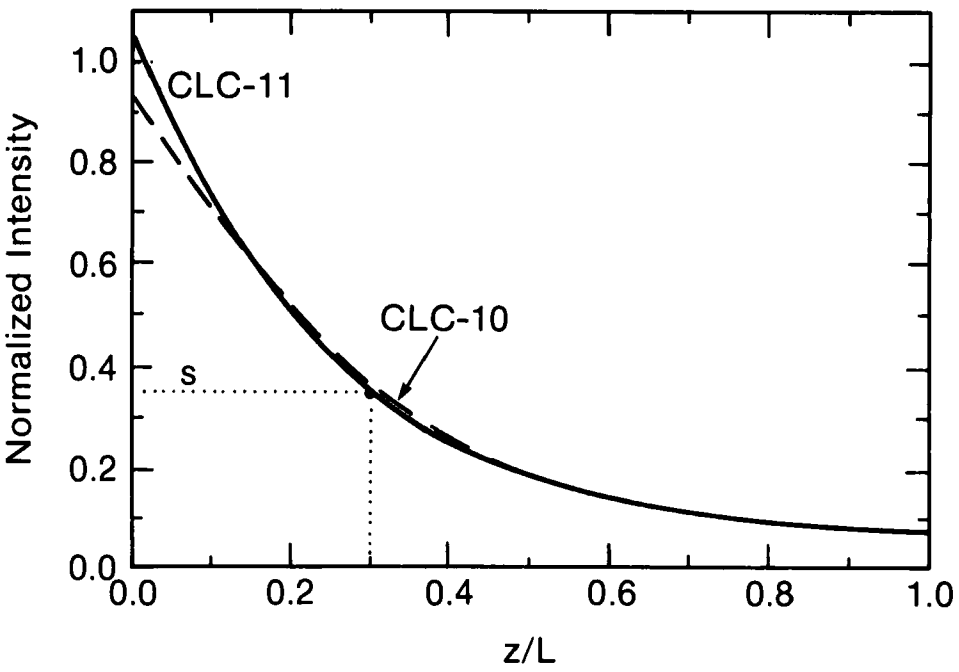

FIGURE 2 Normalized forward propagating field intensity $u(z)$ through the medium for $\kappa L = 2.0$, $q_o L = 10\pi$ at normalized transmitted intensity J = 0.08. Solid lines represent CLC-11 case and dashed lines represent a CLC-10 case.

The relationship between normalized input intensity I and normalized transmitted intensity J for $\kappa L = 2.0$ with $\Delta k/\kappa = 0$ and $q_o L = 10\ \pi$ is shown in Figure 3. For the case of CLC-10, the optical bistability results as predicted by H. G. Winful. However, this nonlinearity disappears in the same range of normalized input intensity I in the case of CLC-11 as expected.

The value of the y component of the director is shown in Figure 4 for the zero field intensity (dashed lines) and for an input intensity which gives rise to the normalized transmitted intensity J = 0.18 (solid lines). This figure shows the pitch dilation near $z = 0$ and the pitch contraction near $z = L$ as we discussed earlier.

The reflectivity R of a CLC cell can be defined by

$$R = \frac{\text{reflected field intensity}}{\text{input field intensity}} = 1 - J/I \tag{34}$$

A plot of reflectivity as a function of the normalized input intensity I is shown in Figure 5 for the two different anchoring conditions. The reflectivity for the CLC-11 is nearly constant over a broad range of normalized input intensity I and differs substantially from that of the CLC-10.

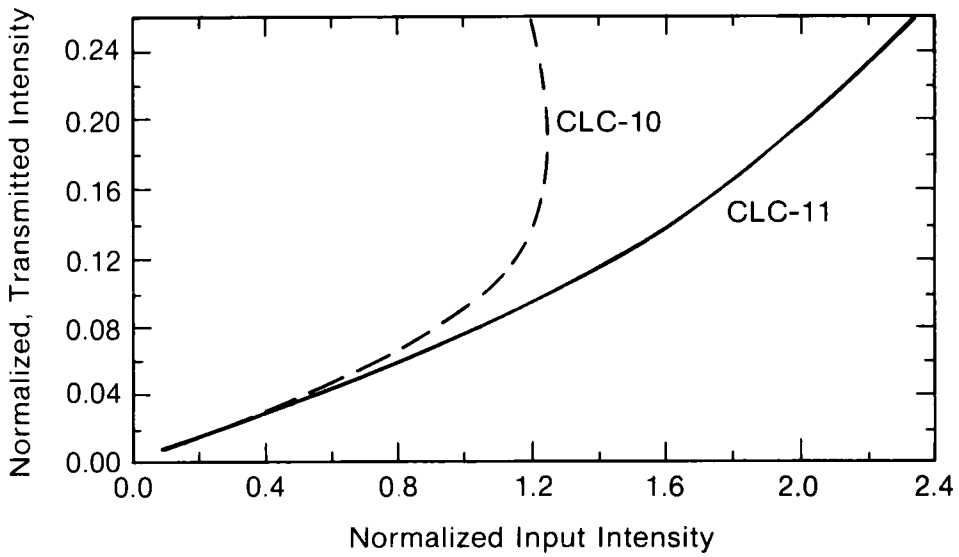

FIGURE 3 Normalized transmitted intensity J versus normalized input intensity I for $\kappa L = 2.0$ (solid lines represent CLC-11 case and dashed lines represent CLC-10 case). Intensities are normalized by $32\pi k_{22}\kappa^2/\epsilon_a$.

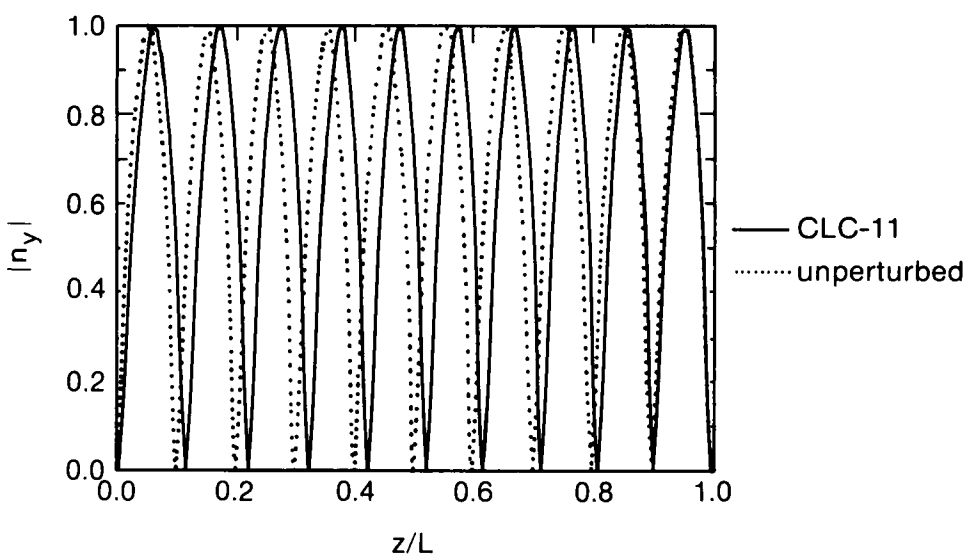

FIGURE 4 The value of the y component of the director for the zero-field case (dashed lines: unperturbed case) and for an incident intensity which causes normalized transmitted intensity J = 0.18 (solid lines). L is chosen to yield an unperturbed $\theta(L) = q_o L = 10\ \pi$.

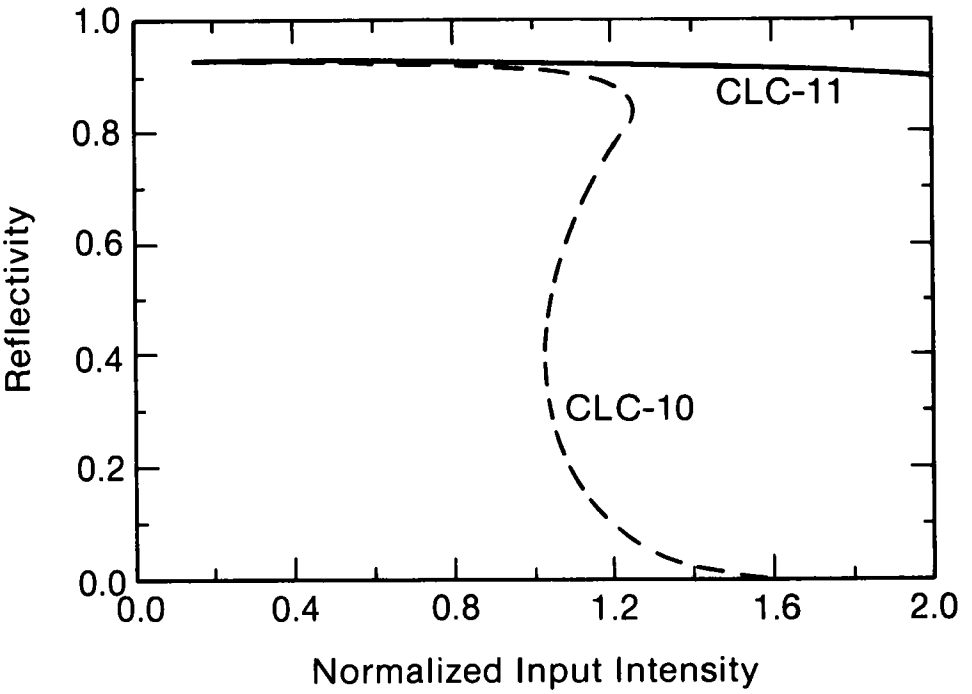

FIGURE 5 Reflectivity R as a function of normalized input intensity I (solid lines represent CLC-11 case and dashed lines represent CLC-10 case).

From Eq. (27), the phase of the reflected field at $z = 0$ can be written as:

$$\phi_-(0) = \phi_+(0) - \cos^{-1}\left[-\sqrt{1 - J/I}\,\{\Delta k/\kappa - 2S + I + J\}\right] \qquad (35)$$

where $I = u(0)$. Equation (35) relates the phase of the reflected field to the normalized input intensity I. The phase of the reflected field for two different anchoring cases as a function of normalized input intensity I and normalized detuning parameter $\Delta k/\kappa$ when $\phi_+(0) = 0$ is shown in Figure 6. Since the strong anchoring at $z = L$ prohibits the helix from changing, the slope of the phase lag in a CLC-10 is steeper than in a CLC-11. Note that for $\Delta k/\kappa = 0$, the phase $\phi_-(0)$ initially starts from 0°. This means that there is no phase shift upon reflection from the CLC in a weak field regime. When $\Delta k/\kappa = 0$, that is, the CLC structure is initially well Bragg-matched, the intense field destroys the Bragg condition as a result of the pitch dilation and contraction and the optical field penetrates more deeply into the CLC before being reflected. Therefore the phase of the reflected field lags as the input intensity increases. When $\Delta k/\kappa > 0$, the pitch of the CLC is already out of the Bragg condition. So the initial phase is less than 0° and decreases further with increasing intensity. When $\Delta k/\kappa < 0$, the incident field forces a pitch dilation and contraction, and the CLC will approach the Bragg condition around

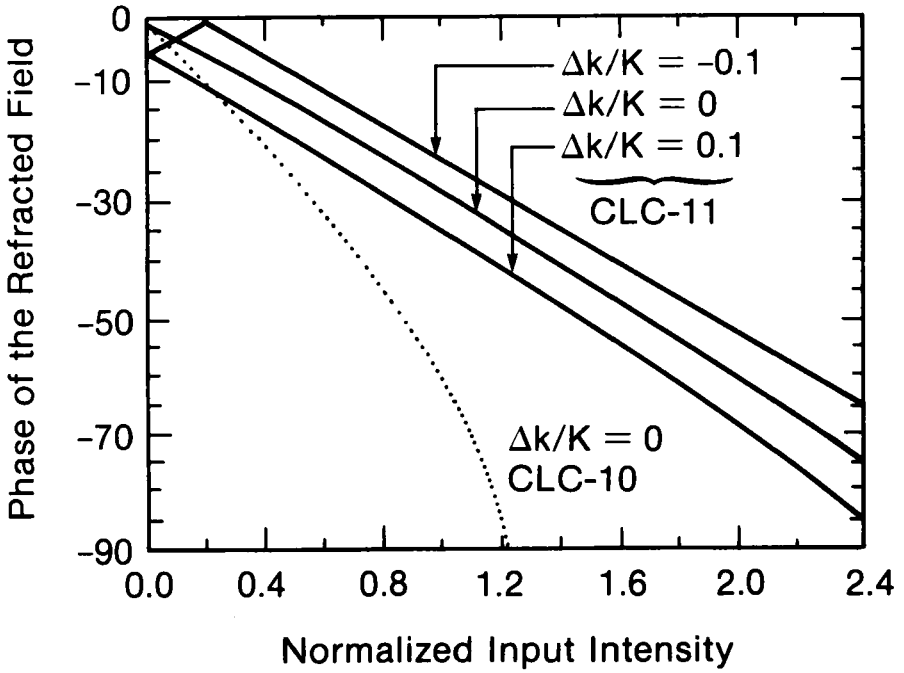

FIGURE 6 Normalized input intensity I versus the phase of the reflected field when the phase of the incident field $\phi_+(0) = 0$ ($\kappa L = 2.0$ with $\Delta k/\kappa = 0, \pm 0.1$ and $q_o L = 10\pi$ for CLC-11: solid lines; $\kappa L = 2.0$ with $\Delta k/\kappa = 0$ for CLC-10: dashed lines).

$z = 0$. Therefore the phase increases until the Bragg condition is met and then decreases. In most cases, pitch dilation is more dominant than pitch contraction because most of the field reflects within a few pitch lengths from $z = 0$.

Now let us consider a plane wave with a Gaussian intensity distribution incident on the CLC. In a first approximation, we can apply our plane wave consideration to study the transverse effects. Several situations are described in Figure 7. When $\Delta k/\kappa < 0$ and the shift of the selective-reflection peak wavelength λ_o ($= n_{av} P_o$) due to the maximum pitch dilation and contraction at the center of the beam is less than the laser wavelength λ_{laser}, the CLC acts as a convex mirror. When $\Delta k/\kappa \geq 0$ and the maximum pitch dilation and contraction are restricted to the selective-reflection band, the phase of the reflected field lags as the intensity increases. Then CLC acts as a concave mirror causing a retro-self-focusing effect. When $\Delta k/\kappa < 0$ and the shifted selective-reflection peak wavelength λ_o is greater than the laser wavelength λ_{laser}, the CLC acts as a combination of concave and convex mirrors. The radius of curvature of the CLC mirror depends on the location of the selective reflection peak wavelength λ_o relative to the laser wavelength λ_{laser} and on the maximum intensity of the incident field.

The right-handed cholesteric liquid crystal with strong surface anchoring at both sides has been used as a laser end mirror to demonstrate the retro-self-focusing

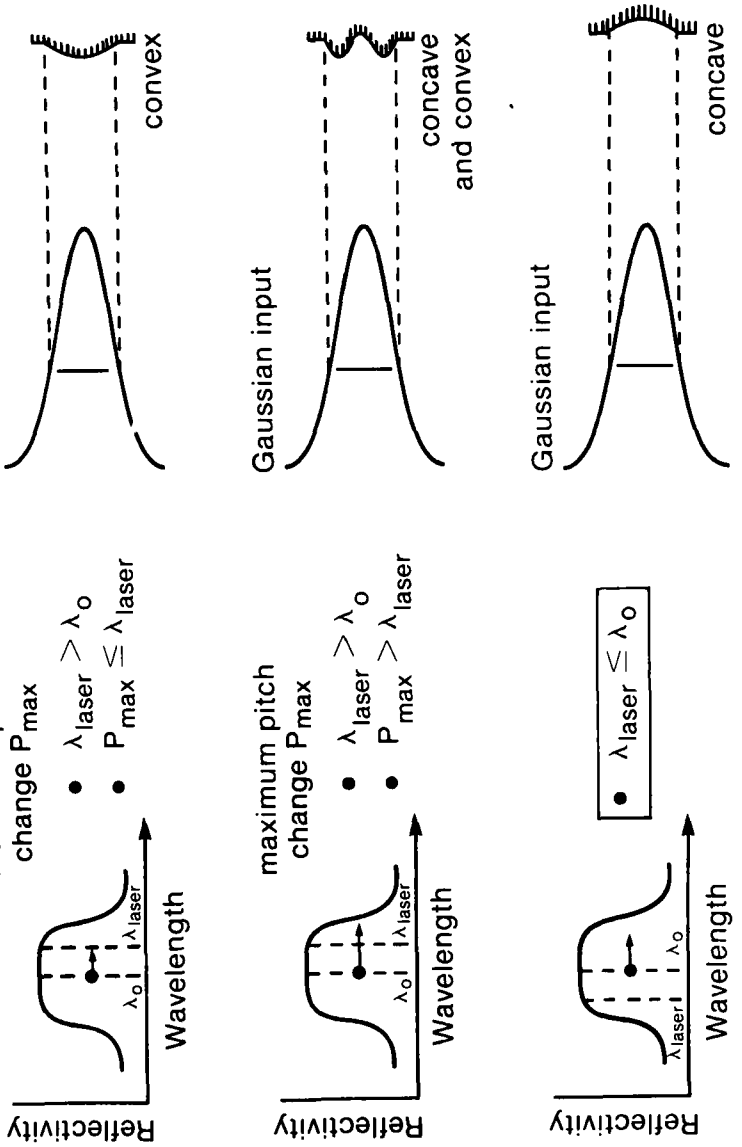

FIGURE 7 The transverse curvature modulation of the CLC-11 mirror by the incident Gaussian intensity distribution for different detuning conditions.

and pinholing effects in our earlier experiment.[6] For the laser end-mirror application, the condition $\lambda_{laser} \leq \lambda_o$ is important because the CLC can be modeled as a concave mirror in this region. When it is used as a laser end mirror, the CLC becomes an active element which changes its radius of curvature in proportion to the intra-cavity intensity.

III. CONCLUSION

We have solved Maxwell's equation and the Euler-Lagrange equation in detail for the cholesteric liquid crystal with strong surface anchoring at both sides (CLC-11). This result shows that pitch dilation at the input side of the cholesteric liquid crystal leads to pitch contraction at the output side. As a result, the slope of the phase lag of the reflected field from the CLC is slower than in a CLC with one-sided, strong surface anchoring at the input side (CLC-10) and the reflectivity is nearly constant over a wide range of input intensities.

Acknowledgments

The authors acknowledge Herbert G. Winful and I. S. Chang for valuable discussions.

This work was supported in part by Daewoo Heavy Industries, Ltd., of Incheon, Korea, the U.S. Department of Energy Office of Inertial Fusion under agreement No. DE-FC08-85DP40200, the New York State Center for Advanced Optical Technology (NYSCAOT), and by the Laser Fusion Feasibility Project at the Laboratory for Laser Energetics which has the following sponsors: Empire State Electric Energy Research Corporation, New York State Energy Research and Development Authority, Ontario Hydro, and the University of Rochester. Such support does not imply endorsement of the content by any of the above parties.

References

1. S. D. Jacobs, *CRC Handbook on Laser Science & Technology Vol. IV, Optical Materials Properties*, Part 2, ed. by M. J. Weber (CRC Press, Boca Raton, FL 1986), pp. 409–465.
2. S. D. Jacobs, K. A. Cerqua, K. M. Marshall, T. J. Kessler, R. J. Gingold, P. J. Laverty and M. Topp, Technical Digest—CLEO '86, THG2, (San Francisco, CA, 1986), pp. 258–259.
3. S. D. Jacobs, K. A. Cerqua, K. L. Marshall, A. Schmid, M. J. Guardalben and K. J. Skerrett, in *Proc. SPIE 895*, presented at OE-Lase '88 (Los Angeles, CA, 10–14 January 1988).
4. H. G. Winful, *Phys. Rev. Lett.* **49**, 1179–1182 (1982).
5. J. C. Lee, S. D. Jacobs and A. Schmid, *Mol. Cryst. & Liq. Cryst.*, **150b**, 617–629 (1987).
6. J. C. Lee, S. D. Jacobs and R. J. Gingold, presentation at the 31st SPIE Annual International Technical Symposium, San Diego, CA, 16–21 August 1987, *Proc. SPIE Vol. 824*.
7. P. G. DeGennes, *The Physics of Liquid Crystals* (Clarendon, Oxford, 1974), pp. 227–229.
8. P. E. Byrd and M. D. Friedman, *Handbook of Elliptic Integrals for Engineers and Scientists* (Springer-Verlag, Berlin, 1971), pp. 120–133.